# Large effective aperture metalens based on optical sparse aperture system

**Tiecheng Liu (刘铁诚)[1,2], Jingpei Hu (胡敬佩)[1,*], Linglin Zhu (朱玲琳)[1], Ruyi Zhou (周如意)[1,2], Chong Zhang (张 冲)[1,2], Chinhua Wang (王钦华)[3], Aijun Zeng (曾爱军)[1,2,**], and Huijie Huang (黄惠杰)[1,2]**

[1]*Laboratory of Information Optics and Optoelectronic Technology, Shanghai Institute of Optics and Fine Mechanics, Chinese Academy of Sciences, Shanghai 201800, China*

[2]*Center of Materials Science and Optoelectronics Engineering, University of Chinese Academy of Sciences, Beijing 100049, China*

[3]*Key Laboratory of Advanced Optical Manufacturing Technologies of Jiangsu Province & Key Laboratory of Modern Optical Technologies of the Ministry of Education, Soochow University, Suzhou 215006, China*

**Corresponding author: hujingpei@siom.ac.cn; **corresponding author: aijunzeng@siom.ac.cn*

Received April 13, 2020; accepted June 1, 2020; posted online July 30, 2020

We present a kind of large effective aperture metalens based on an optical sparse aperture (OSA) system. Each subaperture of the system is a metalens, which is comprised of just a thin Au film with patterned subwavelength rectangular annular arrays on a $SiO_2$ substrate and has a numerical aperture of 0.46 with a diameter of 21.6 μm. Ring6 design was selected to enlarge the effective aperture and enhance the spatial resolution. Compared with the absent mid-frequency and high-frequency modulation transfer function of individual metalens, Ring6 can offer a full-frequency band and show a better restored image quality by using Tikhonov regularization.

*Keywords: optical sparse aperture; metalens; rectangular annular arrays.*

*doi: 10.3788/COL202018.100001.*

Lenses as fundamental elements to imaging systems have traditionally been made in the bulk form by shaping glass or other transparent materials, which hinders their integration in compact optical systems and limits their applications in integrated optics. Recently, the advent of the metalens with ultrathin, lightweight, and tailorable characteristics has attracted intense interest due to their applicability to both consumer [phone cameras, virtual reality (VR)/augmented reality (AR) headsets] and industry products (microscopy, lithography, sensors, and displays)[1–9]. In contrast to traditional lenses, the phase shift of the metalens is determined by the subwavelength geometrical structures rather than relying upon gradual phase accumulation. However, the billions of subwavelength structures of the metalens pose a serious challenge for fabrication, especially for large-area ones.

Most metalenses have so far been fabricated with e-beam lithography, which is with high cost and low process speed not suitable for size scalability. Recently, stepper lithography and imprint lithography also have been used to overcome these limitations[10–14]. However, the exposure field size of the lithography also hinders further enlarging the size of metalenses. Optical sparse aperture (OSA) systems have already been used in telescope optical systems and been designed to obtain the same resolution as a larger filled aperture but with a significant reduction in size and weight by combining the light collected by smaller, individual apertures. Many designs have been proposed and studied, such as Golay, Ring, and Tri-arm sparse aperture designs. This concept is very appealing in technology areas where a filled aperture is too large or hard to fabricate. Sparse aperture concepts have been used to design large astronomical telescopes as well as small endoscopic probes[15–23].

In this Letter, we introduce the OSA system into the metalens imaging system to enlarge the effective aperture and enhance the spatial resolution by using several smaller subaperture metalenses combinations with low cost and easy fabrication. For this purpose, an individual transmitted metalens was proposed, which consists of just a thin Au film with patterned subwavelength rectangular annular arrays on a $SiO_2$ substrate and has a numerical aperture (NA) of 0.46 with a diameter of 21.6 μm. The OSA design of Ring6 was selected to enlarge the effective aperture. The numerical simulation shows that the effective aperture of Ring6 can be almost ten times larger than that of the individual metalens. In addition, compared with the absent mid-frequency and high-frequency modulation transfer function (MTF) of individual metalenses, the MTF of Ring6 can offer a full-frequency band and show a better restored image quality by using Tikhonov regularization.

We have designed a transmission metalens of 21.6 μm diameter, 9.5 μm focal length ($f$), corresponding to a 0.46 NA, and optimized for diffraction-limited focusing in normal incidence at wavelength 1.7 μm ($\lambda$), which is shown in Fig. 1(a). In order to produce the lensing effect, the transmission metalens imposing a spatial profile of phase shifts on the wavefront is satisfied by the following equation:

$$\varphi(x, y) = 2n\pi + \frac{2\pi f}{\lambda} - \frac{2\pi\sqrt{f^2 + x^2 + y^2}}{\lambda}, \qquad (1)$$

 

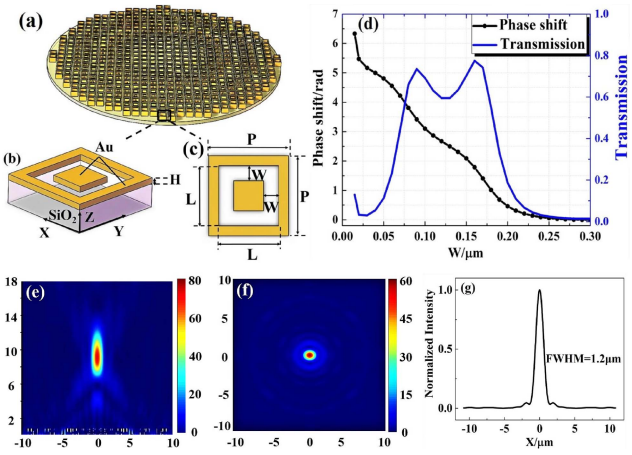


Fig. 1. Metalens structure and corresponding optical properties. (a) Three-dimensional (3D) schematic diagram of the metalens. (b) 3D schematic diagram of rectangular annular element. (c) Top view of rectangular annular element. (d) Optimized results of the transmission (blue line) and phase shift (black dots). (e) Intensity distribution profile of the $X$–$Z$ plane at $y = 0$ μm. (f) Intensity distribution profile of the $X$–$Y$ plane at $z = 9.5$ μm. (g) FWHM of the metalens at a focal point.

where $\lambda$ is the wavelength, $n$ is an arbitrary integer, and $f$ is the focal length. To realize the target phase given by Eq. (1), a structure is comprised of a thin Au film with a patterned subwavelength rectangular annular element on a $SiO_2$ substrate. As seen in Figs. 1(b) and 1(c), the period of the rectangular annular element is $P$. The thickness of Au is $H$, and the width and length of the annular gap are $W$ and $L$, respectively. The numerical simulation was carried out by using the finite difference time domain method (FDTD module, Lumerical Inc.). In this work, the parameters of the proposed structure are fixed: $P = 0.8$ μm, $L = 0.6$ μm, and $H = 0.4$ μm, respectively. Figure 1(d) gives an optimized transmission and phase of the transmission wave as a function of the width of the annular gap at 1.7 μm. By varying the $W$ from 0.015 μm to 0.3 μm, the element was able to produce $2\pi$ phase shift, a 31.35% average transmission, and a 21.06% focusing efficiency. Figure 1(e) shows the light intensity in the $X$–$Z$ plane at $y = 0$ μm. A clear-cut focus appears about 9.5 μm away from the exit surface, which is the basic agreement with our design. Figure 1(f) shows the light intensity in the $X$–$Y$ plane at $z = 9.5$ μm, and the cross section of the focus spot in the $X$ direction is given in Fig. 1(g), indicating a full width at half-maximum (FWHM) of 1.2 μm, which is close to the theoretical diffraction limit of 0.96 μm.

The Ring6 design, as shown in Figs. 2(a) and 2(b), is a design of OSA that combines the light from six individual subaperture metalenses of diameter $d$ separated by a distance $s$ to synthesize a larger aperture. Golay6 and Tri-arm7 are other designs, as seen in Figs. 2(c) and 2(d). For a sparse aperture, the ratio $s/d$ cannot be less than one, because this would cause the subapertures to overlap. The diameter $D$ of a circular aperture is used to calculate effective aperture, which can represent the size of the

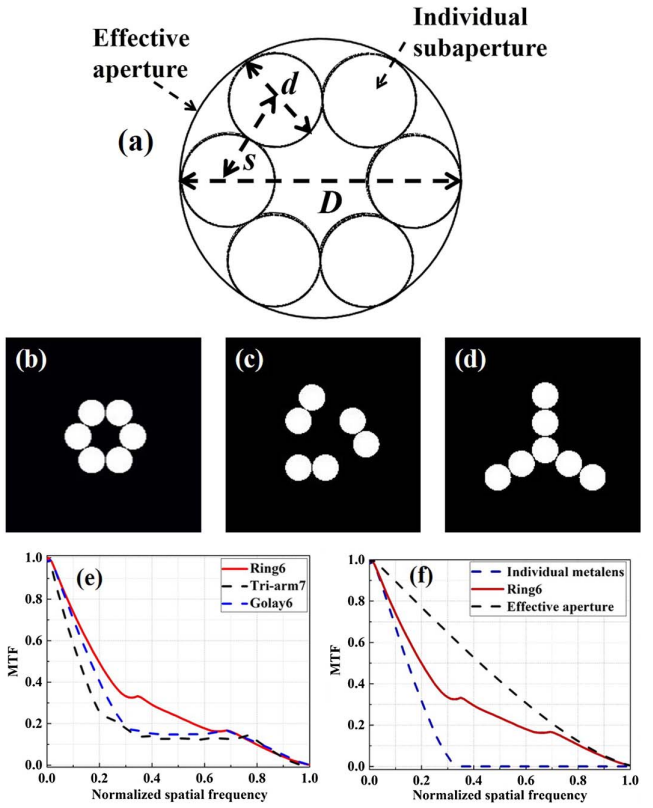


Fig. 2. OSA designs and corresponding MTFs. (a) The Ring6 aperture and parameters in OSA designs. (b) The Ring6 design. (c) The Golay6 design. (d) The Tri-arm7 design. (e) 1D MTF comparison (Ring6, Golay6, and Tri-arm7). (f) 1D MTF comparison (individual metalens, Ring6, effective aperture of Ring6).

aperture that the sparse aperture synthesizes. The fill factor is the total area of the subapertures divided by the effective aperture area and is given by

$$F = Nd^2/D^2, \tag{2}$$

where $N$ is the number of the subapertures. The normalized MTF is calculated by taking a Fourier transform of the point spread function (PSF). For comparison, Fig. 2(e) gives the one-dimensional (1D) normalized MTFs along the frequency axis of three designs (Ring6, Golay6, Tri-arm7), of which the $s/d$ are all equal to one; the low-frequency and mid-frequency MTFs of Ring6 are significantly higher than that of the Golay6 and Tri-arm7 designs, which indicate that a better imaging restoration will be generated. Thus, in the following section, the MTF and corresponding imaging restoration of Ring6 will be investigated. Figure 2(f) gives the 1D normalized MTFs of the three kinds of systems [individual metalens, Ring6 ($F = 64.62\%$, $s/d = 1$), and effective aperture of Ring6]. The MTFs of the different apertures were normalized to the effective aperture of Ring6. As seen in Fig. 2(f), the MTF of individual metalenses drops significantly and zero appears at 0.34 along the frequency axis, resulting in the loss of the mid-frequency and high-frequency of the image. The image quality will be deteriorated.


Fig. 3. The simulated imaging results restored by Tikhonov regularization. (a) Original image. (b) Restored image of individual subaperture. (c) Restored image of Ring6. (d) Restored image of effective aperture of Ring6.

In contrast, the Ring6 system can combine the light captured by subaperture metalenses to capture a higher spatial resolution than possible from any of the individual subapertures[19]. As seen in Fig. 2(f), no zero point appeared in the MTF of Ring6, and the blurred image can be restored by using Tikhonov regularization. As previously mentioned, the diameter of the metalens is 21.6 μm. Thus, the area of the individual metalens and the effective aperture of Ring6 are 366 $\mu m^2$ and $3.47 \times 10^3$ $\mu m^2$. The extension ratio is the effective aperture of Ring6 divided by the individual metalens. The extension ratio of Ring6 ($F = 64.62\%$) is 9.48. As it continues to decrease the fill factors, the extension ratio of Ring6 can be up to 20 until the zero point of the MTF of Ring6 appears.

An imaging process for Ring6 system was simulated and then restored by using Tikhonov regularization. As shown in Fig. 3(a), the cameraman was used as an original image, and the picture size is $256 \times 256$. Figures 3(b)–3(d) show the imaging results restored by Tikhonov regularization of the three kinds of systems (individual metalens, Ring6, and effective aperture of Ring6). As expected, an individual metalens suffers from the size of the aperture, in which a blurred restored image is generated. As a comparison, the restored image quality of Ring6 is significantly better than that of individual metalenses and shows almost the same resolution as the image of the effective aperture of Ring6. The peak signal to noise ratio (PSNR) was used to evaluate the quality of the restored image. The PSNR of the individual metalens is 31.80, and the PSNRs of Ring6 and the effective aperture of Ring6 are 39.07 and 39.40. The PSNR of the Ring6 is higher than that of the individual metalenses and almost equal to the PSNR of the effective aperture of Ring6. Consider the effective aperture of Ring6 as a large size metalens whose area is $3.47 \times 10^3$ $\mu m^2$. As previously mentioned, the area of the individual subaperture is 366 $\mu m^2$, and the area of Ring6 is $2.198 \times 10^3$ $\mu m^2$. Compared with the large size metalens, Ring6 can offer lower fabrication costs and almost the same resolution of restored image as the image resolution of the large size metalens by using Tikhonov regularization. In addition, the larger effective diameter can be obtained by introducing more types of OSA designs.

In conclusion, the OSA system was introduced into the metalens imaging system to enlarge the effective aperture and enhance the spatial resolution by using several smaller subaperture metalens combinations with low cost and easy fabrication. For this purpose, an individual transmitted metalens was proposed, which consists of just a thin Au film with patterned subwavelength rectangular annular arrays on a $SiO_2$ substrate and has an NA 0.46 with a diameter of 21.6 μm. The OSA design of Ring6 was selected, and the numerical simulation shows that the effective aperture of Ring6 can be almost ten times larger than that of the individual metalens. In addition, compared with the absent mid-frequency and high-frequency MTF of individual metalenses, the MTF of Ring6 can offer a full-frequency band and show a better restored image quality by using Tikhonov regularization. This method can be used to promote the application of metalenses in VR devices or biological imaging techniques.

This work was partially supported by the Intergovernmental International Cooperation Program in Science and Technology Innovation (No. 2016YFE0110600), International Science & Technology Cooperation Program of Shanghai (No. 16520710500), National Natural Science Foundation of China (No. 61805264), Youth Innovation Promotion Association CAS, Science and Technology Commission of Shanghai Municipality (No. 17YF1429500), Shanghai Sailing Program (No. 18YF1426500), and University Scientific Research Foundation of Jiangsu Province (No. KJS1713).

## References

1. J.-S. Park, S. Zhang, A. She, W. T. Chen, P. Lin, K. M. A. Yousef, J.-X. Cheng, and F. Capasso, Nano Lett. **19**, 8673 (2019).
2. A. V. Kildishev, A. Boltasseva, and V. M. Shalaev, Science **339**, 1232009 (2013).
3. A. Arbabi, Y. Horie, M. Bagheri, and A. Faraon, Nat. Nanotechnol. **10**, 937 (2015).
4. W. T. Chen, A. Y. Zhu, V. Sanjeev, M. Khorasaninejad, Z. Shi, E. Lee, and F. Capasso, Nat. Nanotechnol. **13**, 220 (2018).
5. W. T. Chen, A. Y. Zhu, J. Sisler, Y.-W. Huang, K. M. A. Yousef, E. Lee, C.-W. Qiu, and F. Capasso, Nano Lett. **18**, 7801 (2018).
6. M. Khorasaninejad and F. Capasso, Science **358**, eaam8100 (2017).
7. N.-F. Yu, P. Genevet, M. A. Kats, F. Aieta, J.-P. Tetienne, F. Capasso, and Z. Gaburro, Science **334**, 333 (2011).
8. R. Sawant, P. Bhumkar, A. Y. Zhu, P. Ni, F. Capasso, and P. Genevet, Adv. Mater. **31**, 1805555 (2019).
9. Y. Cui, G. X. Zheng, M. Chen, Y. L. Zhang, Y. Yang, J. Tao, T. T. He, and Z. L. Li, Chin. Opt. Lett. **17**, 111603 (2019).

10. G.-Y. Lee, J.-Y. Hong, S. H. Hwang, S. Moon, H. Kang, S. Jeon, H. Kim, J.-H. Jeong, and B. Lee, Nat. Commun. **9**, 4562 (2018).
11. A. She, S. Y. Zhang, S. Shian, D. R. Clarke, and F. Capasso, Opt. Express **26**, 1573 (2018).
12. G. Brière, P. Ni, S. Héron, S. Chenot, S. Vézian, V. Brändli, B. Damilano, J.-Y. Duboz, M. Iwanaga, and P. Genevet, Adv. Opt. Mater. **7**, 1801271 (2019).
13. Z.-B. Fan, Z.-K. Shao, M.-Y. Xie, X.-N. Pang, W.-S. Ruan, F.-L. Zhao, Y.-J. Chen, S.-Y. Yu, and J.-W. Dong, Phys. Rev. Appl. **10**, 014005 (2018).
14. T. Hu, C.-K. Tseng, Y. H. Fu, Z. J. Xu, Y. Dong, S. J. Wang, K. H. Lai, V. Bliznetsov, S. Y. Zhu, Q. Y. Lin, and Y. D. Gu, Opt. Express **26**, 19548 (2018).
15. A. B. Meinel, Appl. Opt. **9**, 2501 (1970).
16. J. D. Monnier, Rep. Prog. Phys. **66**, 789 (2003).
17. S.-J. Chung, D. W. Miller, and O. L. de Weck, Proc. SPIE **4849**, 181 (2002).
18. J. R. Fienup, Proc. SPIE **4091**, 43 (2000).
19. R. D. Fiete, J. A. Mooney, T. A. Tantalo, and J. R. Calus, Proc. SPIE **4091**, 64 (2000).
20. R. D. Fiete, T. A. Tantalo, J. R. Calus, and J. A. Mooney, Opt. Eng. **41**, 1957 (2002).
21. N. J. Miller, M. P. Dierking, and B. D. Duncan, Appl. Opt. **46**, 5933 (2007).
22. C. H. Zhou and Z. L. Wang, Opt. Express **26**, 6973 (2018).
23. Z. L. Xie, H. T. Ma, B. Qi, G. Ren, J. L. Shi, X. J. He, Y. F. Tan, L. Dong, and Z. P. Wang, Chin. Opt. Lett. **15**, 041101 (2017).